Journal of Computational Chemistry & Molecular Modeling (ISSN: 2473-6260)

Graphyne: Optical Excitations and Charge Distributions

DOI: 10.25177/JCCMM.6.1.RA.10839

Research

Accepted Date: 20th Oct 2023; Published Date:10th Nov 2023

Andreas Ø. Madsen, Sophia V. K. Mikkelsen, and
Kurt V. Mikkelsen

♦ Department of Chemistry, University of Copenhagen, Copenhagen, DK-2100, Denmark

CORRESPONDENCE AUTHOR
Kurt V. Mikkelsen,
E-mail: kmi@chem.ku.dk

CITATION
Kurt V. Mikkelsen, Graphyne: Optical Excitations and Charge Distributions (2023) Journal of Computational Chemistry & Molecular Modeling 6(1) p:663-676

ABSTRACT
Graphyne is the new wonder material and the optical transitions and charge distributions of different graphyne fragments are investigated using density functional theory calculations.

Keywords: Graphyne, optical transitions, charge distributions, density functional theory.

1. INTRODUCTION

History has clearly shown that mankind has pursued an ever increasing urge for finding new technological solutions to the many problems that have been encountered and daily encounter around the world. This rush results in more and more innovative solutions in order to be the first to find the next ”big thing”. Recently, graphene has been the focus of an innovative discovery. It was originally discovered theoretically in 1947,[1] but it was first extracted from graphite as a single atomic layer in 2004.[2] Graphene has for a long time been known as the ”wonder material” due to its large range of applications. Below is a list of some of the different possible applications that can be made by the use of mono layer graphene:[3]

- Touchscreens
- Composites
- Sensors
- Energy Storage Devices
- Barrier Films
- Optics
- Medicine e.g. drug delivery

These are only some selected applications. Mono layer graphene is not easy to utilize in practical applications, yet there are still many papers being published each year about graphene and the utilization of the material. Looking at the number of publications each year containing graphene as a key word, the number has increased over the years since it was first extracted from the graphite crystal[4]. A majority of the articles concern the properties of graphene, with a secondary focus on the application, which indicates that the properties at that time were sufficiently assessed [5].

Graphene consist of a mono layer of sp^2 hybridized carbon atoms, and the carbon atoms are arranged in a 2D honeycomb lattice structure resulting in a delocalization of the electrons in the graphene sheet. Some of the properties that follow from this unique construction are[6]:

- High fracture strength
- Excellent electrical and thermal conductivity
- Fast mobility of charge carriers ($2 \times 10^5\, cm^2/V\, s$)
- Large specific surface area
- Biocompatibility
- Tunable band gap [5]

The electro-chemical aspects of graphene are in very high course, as we today more than ever search for new and greener ways to obtain and store energy. Since graphene has a large surface area and excellent chemical stability, while having a high electrochemical activity, it performs well as a metal free electro catalyst for fuel cells [7, 8]. Furthermore, it shows promising features for energy storage and electric charges in super capacitors[9] and lithium batteries [10]. A remarkable compatibility between graphene and transition metals, metal oxides and conducting polymers shows a promising way to produce high-performance graphene-based materials or composites (GBM) [11]. A mono layer is not the only configuration of graphene, it is possible to stack the graphene layers making double layer graphene, triple layer graphene, etc. The layer can furthermore be rolled into 1D carbon nanotubes (CNT’s), wrapped up into 0D fullerene or simply stacked as mentioned into 3D graphite [12].

Graphyne, which is studied in this presentation, is another predicted allotrope of carbon, instead of being sp^2 hybridized like graphene, graphyne has sp triple bound carbons making a $sp - sp^2$ hybridized 2D lattice [13]. In order to get this type of hybridized carbon-carbon bonds there is formed acetylene bonds, resulting in a several version of graphyne. The notation of graphyne changes depending on the length of the carbon chain between each benzene ring, thus graphyne-1, graphyne-2, etc. [14].

Graphyne mono layers have many of the same properties as graphene, which are still to be determined, but the nature of the $sp - sp^2$ bonds allows from some interesting features. One of these is the strain engineering of Dirac cones, which Wang et al. [15]

managed by using 6,6,12-graphyne to make two kinds of non-equivalent anisotropic Dirac cones in the first Brillouin zone. By changing the uniaxial compressive strain that is applied to graphyne the Dirac cones can be tuned individually resulting in a self-doping effect.

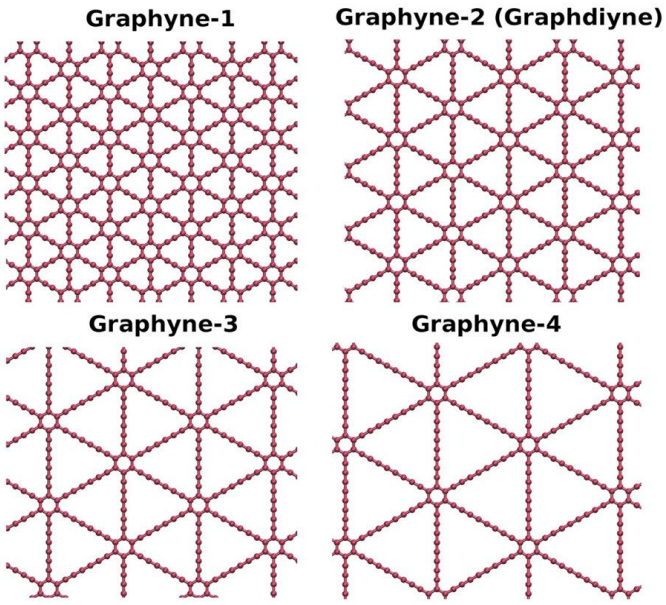

Figure 1: Graphyne types, from Ozmaian et al. [14]

We focus on the oligomers that were synthesized by Kilde et al. [16] as model compounds for 6,6,12graphyne, Figure 2. These five proposed model compounds for the synthesis of 6,6,12-graphyne, will be theoretically studied by the use of Density-Functional Theory (DFT). We investigate the properties of each model compound by calculating excitation energies for each combination of the five compounds as well as the individual compound. We ensure that the calculations are as accurate as possible within reasonable CPU capacity by performing a benchmark study with a range of relevant basis sets and functionals for DFT calculations.

Previously, theoretical investigations have shown that graphyne just as with graphene will be suited as redox catalyst for fuel cells [17]. Therefore it is important to perform calculations of the charge distributions for the respective charged graphyne model compounds.

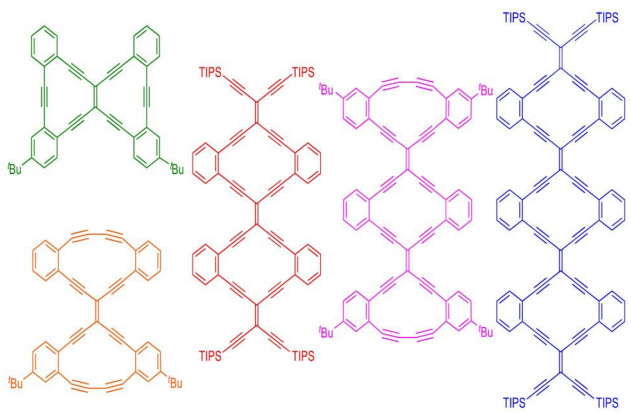

Figure 2: Graphyne segments synthesized by Kilde et al. [16]

2. Benchmark

For the DFT investigations we have selected the following five functionals: *B3LYP*, *CAM-B3LYP*, *APFD*, *M062-X* and *ωB97X-D*. We have utilized the following basis sets: *6-31G(d,p)*, *6-311G(d,p)* and *6-311+G(d,p)*.

Going from the green to the blue segment (see Figure 2) there is a major increase in the sizes of the molecular systems and we limit our benchmark investigation to the green and the red systems. We compare the calculated absorption spectra to an experimental absorption band measured by Kilde et al. [16] and the experimental spectra are shown in Figure 3. The experimental absorption spectra are performed in dichloromethane (DCM) and we investigate the solvent effects on the spectra by performing separate geometry optimizations and excitation calculations for the orange segment in DCM. The segment is geometrically optimized with the basis-set 6-311*G*(*d,p*), while the time-dependent density functional (TD-DFT) calculation itself is carried out with the basis-set 6-311+*G*(*d,p*). Both the geometric and the TD-DFT calculations are done in the solvent DCM[18]. Comparing the theoretically calculated absorption bands in Fig. 4 with the experimentally measured band in Fig. 3 (*Orange Curve*), it is clear from the 500-600 nm band that both *B3LYP* and *APFD* overestimate the wavelength. The absorption band experimentally measured at 250-300 nm, does however match better for *APFD* and *B3LYP* than with the other three func-

tionals. Despite this the ratio between the peaks are off, compared to *CAM-B3LYP*, *ωB97X-D* and M062 -X. *CAM-B3LYP*, *ωB97X-D* and M062-X all contain a type of long-ranged exchange correlation, which for larger molecules is important. This results in *CAM-B3LYP* outperforming *B3LYP* in most scenarios[20]. M062-X, *CAM-B3LYP* and *ωB97X-D* all perform very well[21], but have different computational requirements. Due to this CAM-B3LYP was the chosen functional for the remaining calculations, both for the geometric optimization and excitation calculations, as to reduce the computational load. We have chosen the basis set 6-311*G*(*d,p*) for the geometry optimizations and the basis set 6-311 + *G* (*d,p*) for the calculations of excitation energies.

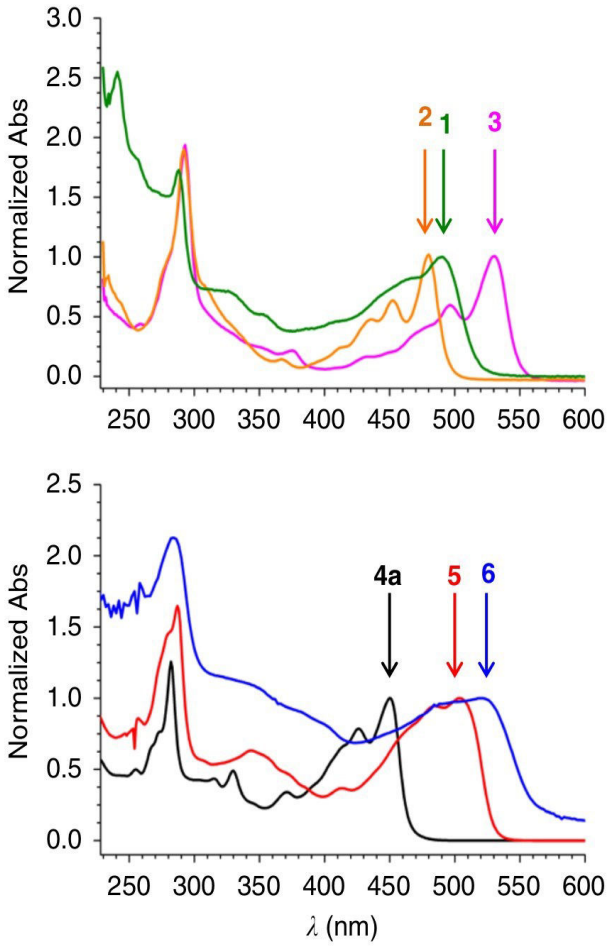

Figure 3: Absorption intensities for the different Graphyne-segments, measured by Kilde et al. [16] in THF.The colors of the curves match with the color tag for each of the segments.

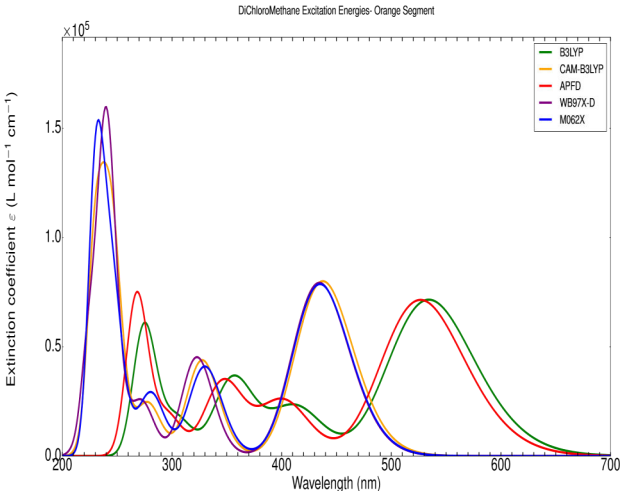

Figure 4: Excitation energies for the *orange segment* with different functionals, plotted through a gaussian distribution[19]. All the calculations are carried out with the basis-set 6-311 + *G*(*d,p*) and the solvent is *(DCM)*[18].

3. Individual Segments

Each of the five segments was geometrically optimized by the use of *CAM-B3LYP* and 6-311*G*(*d,p*), while the excitation energies were calculated with *CAM-B3LYP* and 6-311+*G*(*d,p*) to ensure that sufficiently high accuracy was obtained.

Regarding the absorption spectra of the different single segments presented in Fig. 5 and 6, a red-shift is observed as the size of the segment increases.

The green segment only produces one clear absorption band located at (200-350 nm), while there is a band at 450-600 nm, which is not very clear. the 200-350 nm band can be located for the other segments as well. For the orange segment and red segment the band is split into two, where the first band is slightly blue-shifted, while the other is slightly red-shifted giving a larger absorption span. Furthermore, there is a clear representation of the band from 500-600 nm observed on the green segment, whereas for the orange segment (Fig. 5c) it is blue-shifted ranging from 380-500 nm, and for the red segment (Fig. 5e) a wide absorption band from 400-600 nm is observed. Increasing the size further to the purple segment (Fig. 6a) the absorption intensity is lowered for the

first band, while maintaining the 400-600 nm band that was observed for the orange and red segments. The blue segment (Fig. 6c) recovers some of the original peak intensity, while gaining a small band at 300-400 nm. Lastly the large band observed at 400-600 nm for the purple segment is slightly red-shifted.

Segment	Partial Charge Range
Green	0.386 to 0.383
Orange	0.352 to 0.352
Red	0.496 to 0.496
Purple	0.412 to 0.412
Blue	0.501 to 0.501

Table 1: The ranges of the partial charges of the charge distributions for the different segments

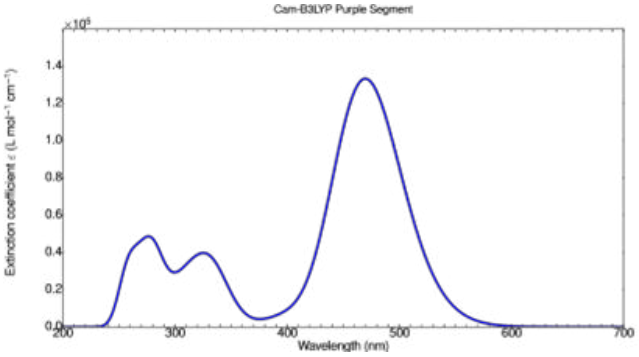

(a) Excitation energies for the *green segment* calculated with *CAM-B3LYP and* 6-311 + *G*(*d, p*) using Gaussian[18], plotted through a gaussian distribution[19].

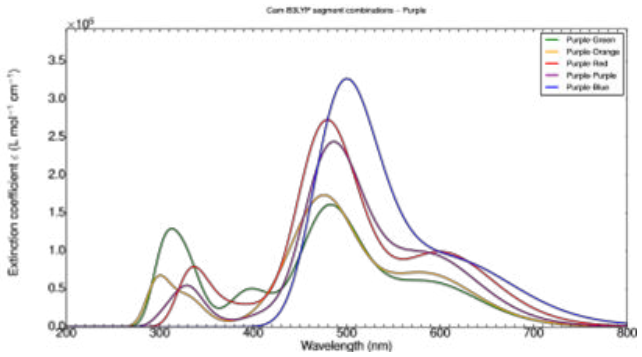

(b) Excitation energies for all segments combinations containing the *green segment*, calculated with *CAMB3LYP* and 6-311+*G*(*d, p*) using Gaussian[18], plotted through a gaussian distribution[19].

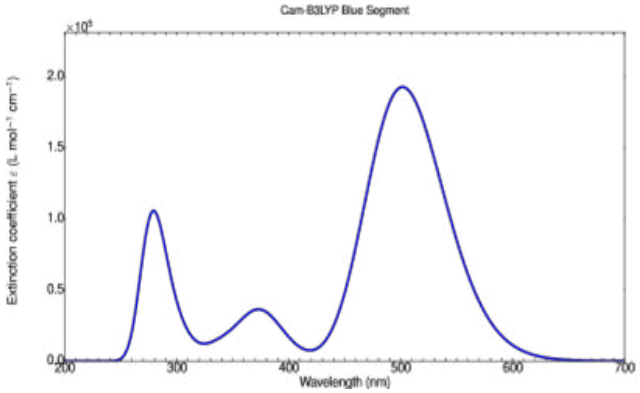

(c) Excitation energies for the *orange segment* calculated with *CAM-B3LYP* and 6-311 + *G*(*d, p*) using Gaussian[18], plotted through a gaussian distribution[19].

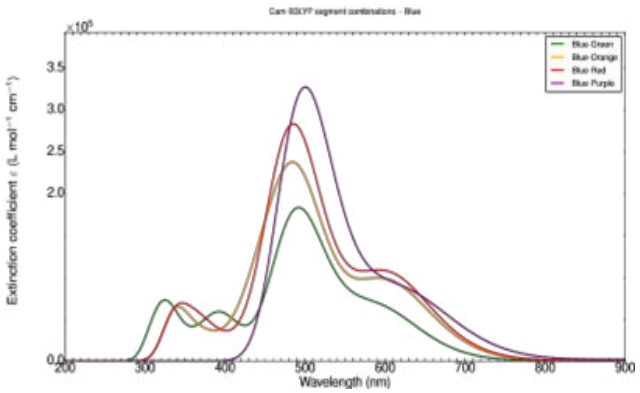

(d) Excitation energies for all segments combinations containing the *orange segment*, calculated with *CAMB3LYP* and 6-311+*G*(*d, p*) using Gaussian[18], plotted through a gaussian distribution[19].

Figure 5: Left-hand side: Excitation energies for single segments.

Right-hand side: Excitation energies for combined segments

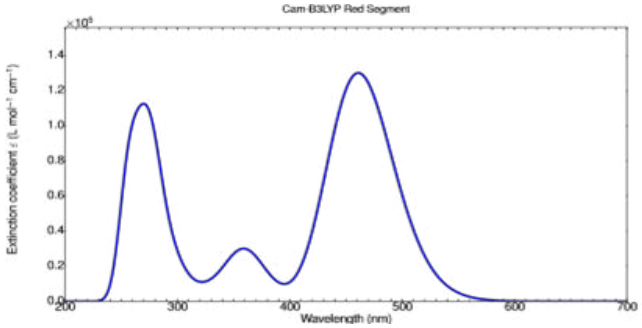

(e) Excitation energies for the *red segment* calculated with *CAM-B3LYP* and 6-311 + *G*(*d, p*) using Gaussian[18],
plotted through a gaussian distribution[19].

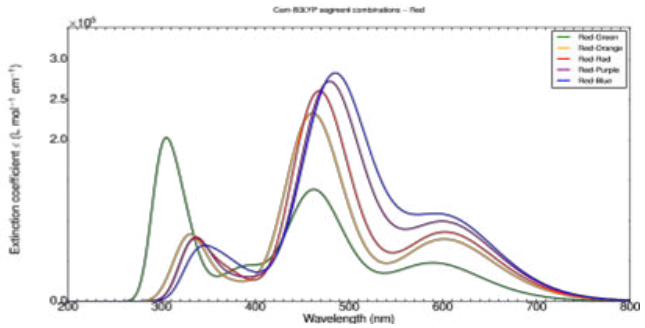

(f) Excitation energies for all segments combinations containing the *red segment*, calculated with *CAM B3LYP* and 6-311+*G*(*d, p*) using Gaussian [18],plotted through a gaussian distribution[19].

Figure 5: Left-hand side: Excitation energies for single segments.

Right-hand side: Excitationenergies for combined segments

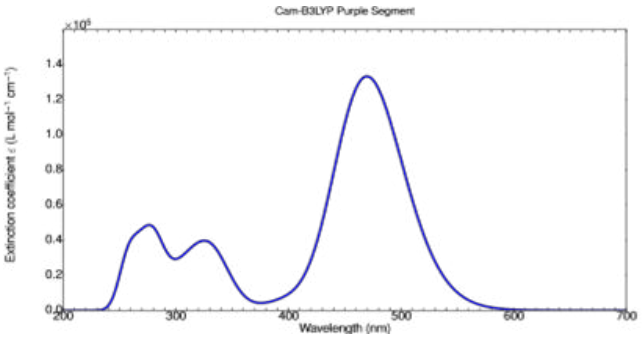

(a) Excitation energies for the *purple segment* calcu- lated with *CAM-B3LYP* and 6-311 + *G* (*d, p*) using Gaussian[18], plotted through a gaussian distribution[19].

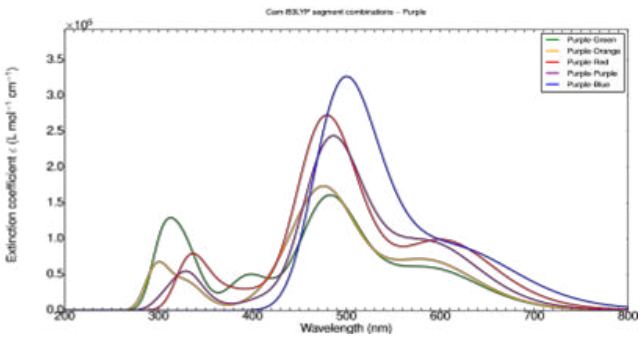

(b) Excitation energies for all segments combinationscontaining the *purple segment*, calculated with *CAMB3LYP* and 6-311+*G*(*d, p*) using Gaussian[18], plotted through a gaussian distribution[19].
plotted through a gaussian distribution[19].

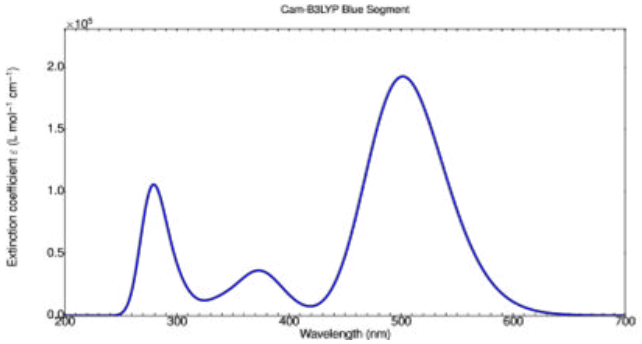

(c) Excitation energies for the *blue segment* calculated with *CAM-B3LYP* and 6-311 + *G*(*d, p*) using Gaussian[18], plotted through a gaussian distribution[19].

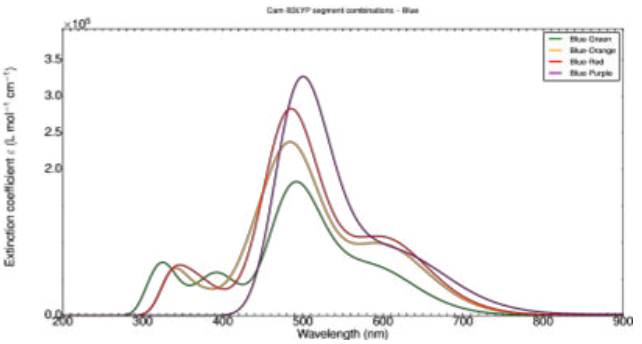

(d) Excitation energies for all segments combinations containing the *blue segment*, calculated with *CAMB3LYP* and 6-311+*G*(*d, p*) using Gaussian[18], plotted through a gaussian distribution[19].
plotted through a gaussian distribution[19].

Figure 6: Left-hand side: Excitation energies for single segments.

Right-hand side: Excitation energies for combined segments

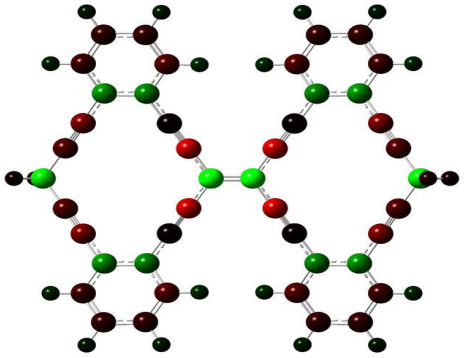

Figure 7: Molecular structure of the orange Segment with APT partial charges ranging from -0.352 to 0.352. Green represents a partial positive charge, red represents a partial negative charge and black represents a partial neutral charge

4. Combined Segments

As each of the segments are building blocks for the Graphyne sheet, an investigation of the optically properties when combining the segments in pairs of two were performed. By combining the segments lengthwise, it lead to 15 different combinations, taking the scenarios where two identically segments were combined into account as well.

Since there was observed a very small change in the thermal corrected energies between the three basis-sets, the geometric optimizations of the combined segments were done with the smaller basis-set 6-31*G*(*d,p*) and the functional CAM-B3LYP thereby saving computational efforts. For excitation energies the 6-311*G* (*d,p*) basis-set was used along with the CAM-B3LYP functional[18].

As observed for the single segments an increase in the molecular size results in a red-shift of the absorption bands. We observed the same for the combined segments when comparing with the single segment for each case (green and green-green, orange and orange-orange etc). When increasing the original segment size, the effect of combining the segment with other segments is again that a larger structure induces a larger red-shift. In Fig. 5b we note that the green-green segment (green curve) is red-shifted. When the combination is changed to a green-orange (orange curve), this trend is observed again as the green segment is combined with larger segments. Figure 6d shows very clearly that the absorption bands are red-shifted as the molecular sizes of the segments are increased.

Comparing the absorption spectra for the green segment and the green-green combination seen in Figure 5b, a red shift and narrowing of the peak of the green segments at 200-350nm is observed.
In addition to the first band, a second contribution is observed at 380-490 nm, while the band at 500-600 nm for the single segment is now increased in both intensity and width.

The same trend is seen for the orange segment, where the orange-green combination results in a large red-shift and intensity increase as seen in Figure 5d. Introducing the orange-orange combination does not only provide a red-shift again, but also a further increase in the intensity of the 400-500 nm absorption band.

When making combinations from a red, purple or blue segment we observe that the red-shifts increase but the changes in the red-shift become smaller as the segments get larger (see Fig.6). Therefore the red-orange and red-blue segment combinations, only induce a slight change in comparison to each other.

5. Charge Population

Both Graphyne and Graphene consist of carbons mainly connected through sp/sp^2 hybridization, thus allowing for de-localization of the electrons throughout the molecule. Therefore, the charge populations of the molecules are worth investigating. Graphene consists of carbon bonds with sp^2 hybridization with connections throughout the

the whole molecular sheet. However, graphyne does not have this but instead it contains *sp* hybridization on some of the carbon-carbon bonds.

The charge populations are obtained from the geometric optimizations using the density functional $\omega B97X$-D and the basis set 6-311$G(d,p)$[18]. For the green segment in Figure 10 we observe that the partial positive charge is pushed towards the centre of the molecule, thus onto the two carbons in the middle bonded by a sp^2-sp^2 double bond. The partial negative charge is, however, also pushed towards the centre, but is instead located on the four carbons with a *sp*-*sp* triple bond to a partial neutral carbon and a sp^3-sp^3 to the positive centre carbons.

Increasing the size of the segment lengthwise from the green segment to the blue segment, the same trend is observed. Once again the negative charge is located on the *sp* hybridized carbons and then partial positive charge on the sp^2 hybridized centre carbons, with the exception of the ends of the segment where the hydrogen atoms obtain a partial positive charge instead of the carbon atom. Introducing the ”loose” triple bond carbon-carbon ends results in a larger partial charge distribution in the molecule, which can be seen from comparing the red, purple and blue segments. With their respective -0.496 to 0.496, -0.412 to 0.412, and -0.501 to 0.501 partial charge distributions.

If the same partial charge behaviour can be assumed for the sheet version of the Graphyne segments, Graphyne would differ significantly from the charge population of Graphene. Graphene tends to push the partial charges out from the centre to the edge of the molecule, balancing the positive and negative partial charge on the hydrogen and carbon at the edge, rather than on the centre atoms.

5.1. Addition of External Charge to the System

To further investigate the charge properties and the conjugation throughout the Graphyne segments external charges were applied to the system. To verify that the adding of a charge of either positive or negative sign would produce the same tendencies, two scenarios are made for the red and blue segments. In the first scenario a charge of -2 was applied to the system, while for the second scenario a charge of +2 was applied. We consider the charge populations involving different charges of the segments. Applying a charge of -2 to the system of the red segment, and we can then compare the charge distribution in Figure 12 with the partial charged case on Figure 8. The relative size of the charge distribution remains in the same area, while the charge is pushed away from the center plane. As such the double bonded carbons in the center plane are now nearly neutral, while the benzene rings have accepted some of the positive and negative charge instead. The hydrogen atoms connected to the ends of the alkyne groups on both sides of the structure have once again accepted a positive partial charge to counter the negative charge on the carbon connected to it. Switching the charge to a positive charge of +2 results in several changes to the charge placement. Comparing the +2 charge scenarios in Figure 13 with the other red segment scenarios, charges are now again placed in the centre plane. Some of the behaviour for the neutral red segment is thus restored when adding a positive charge to the system. The specific charge placement is shifted by one carbon, and the relative size of the charge distribution is reduced to +/- 0.317. It should be noted that the charge is moved to the benzene rings on the positive charged scenario too, so the charge is mostly delocated for the positive charged case.

To study this tendency further the same charge scenarios were applied to the red segment. The blue segment also has the open alkyne group ends and was thus expected to show the same tendencies. Fig. 14 exhibits the same tendency for the negative scenario, where the charge once again is removed from the centre plane and moved to the benzene rings and the hydrogen atoms still carry an partial positive charge. Regarding the size of the charge distribution it is once again very similar to the partial case presented in Figure 11. Adding a positive charge of +2, as seen on Figure 15, results in a more de-localized charge distribution with a range of +/- 0.426. Once again the carbons in the centre plane carry a positive charge as seen for the partial charged case.

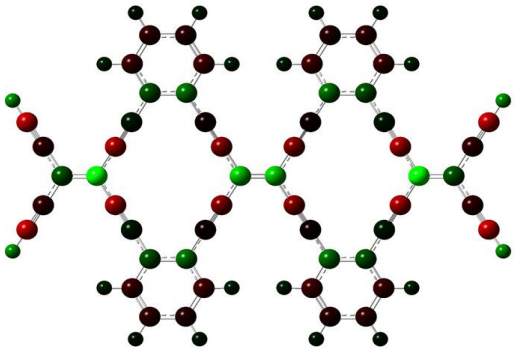

Figure 8: Molecular structure of the red segment with APT partial charges ranging from -0.496 to 0.496. Green represents a partial positive charge, red represents a partial negative charge and black represents a partial neutral charge

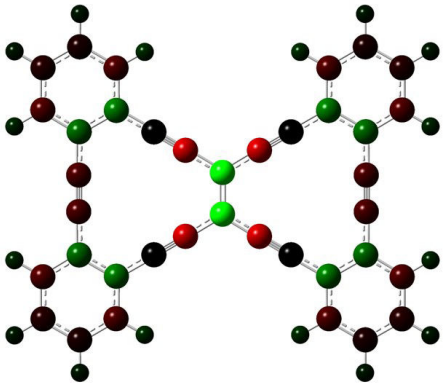

Figure 10: Molecular structure of the green segment with APT partial charges ranging from -0.386 to 0.383. Green represents a partial positive charge, red represents a partial negative charge and black represents a partial neutral charge

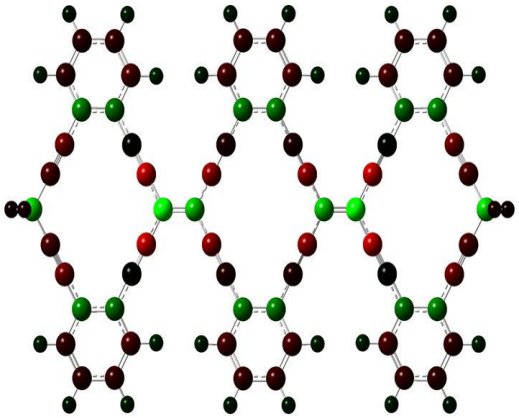

Figure 9: Molecular structure of the purple segment with APT partial charges ranging from -0.412 to 0.412. Green represents a partial positive charge, red represents a partial negative charge and black represents a partial neutral charge.

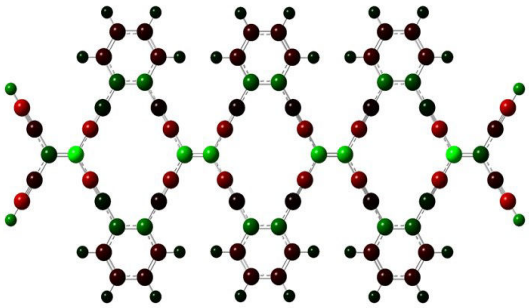

Figure 11: Molecular structure of the blue segment with APT partial charges ranging from -0.501 to 0.501. Green represents a partial positive charge, red represents a partial negative charge and black represents a partial neutral charge.

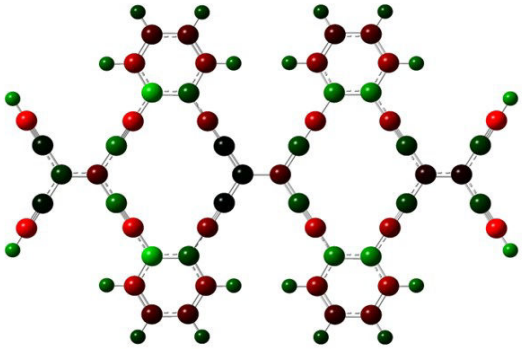

Figure 12: Molecular structure of the red segment with ESP with the addition of -2 charge ranging from -0.553 to 0.553. Green represents a partial positive charge, red represents a partial negative charge and black represents a partial neutral charge.

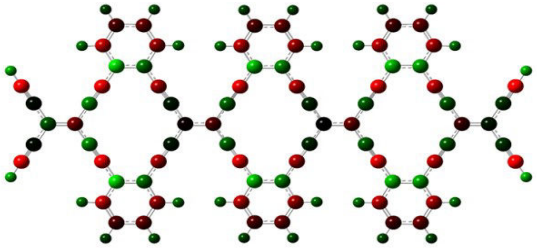

Figure 14: Molecular structure of the blue segment with ESP with the addition of -2 charge ranging from -0.507 to 0.507. Green represents a partial positive charge, red represents a partial negative charge and black represents a partial neutral charge.

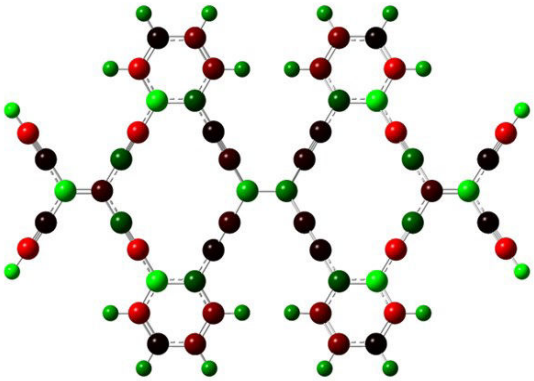

Figure 13: Molecular structure of the red segment with ESP with the addition of +2 charge ranging from -0.317 to 0.317. Green represents a partial positive charge, red represent a partial negative charge and black represents a partial neutral charge.

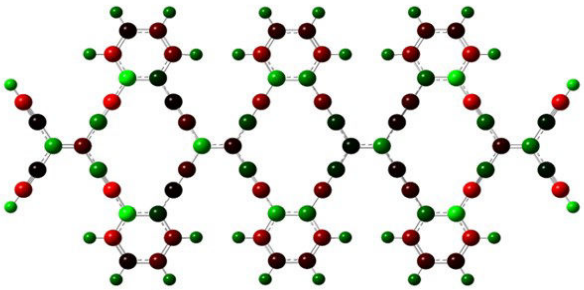

Figure 15: Molecular structure of the blue segment with ESP with the addition of +2 charge ranging from -0.426 to 0.526. Green represents a partial positive charge, red represents a partial negative charge and black represents a partial neutral charge.

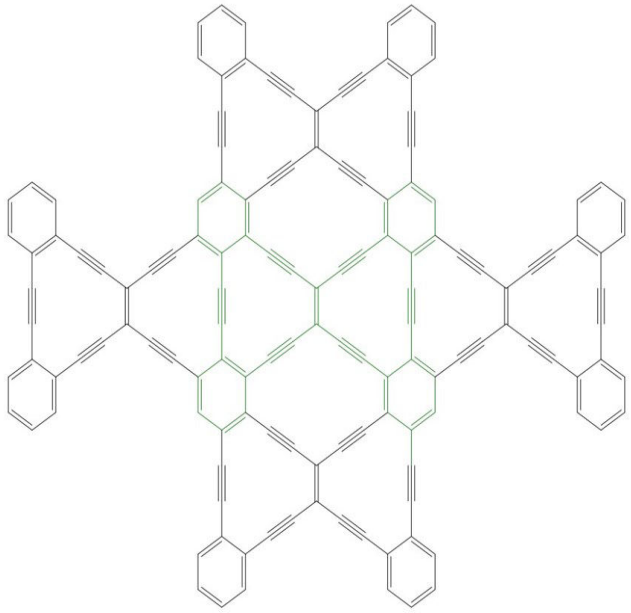

Figure 16: The proposed structure of the Graphyne ”Flake” based upon the green segment

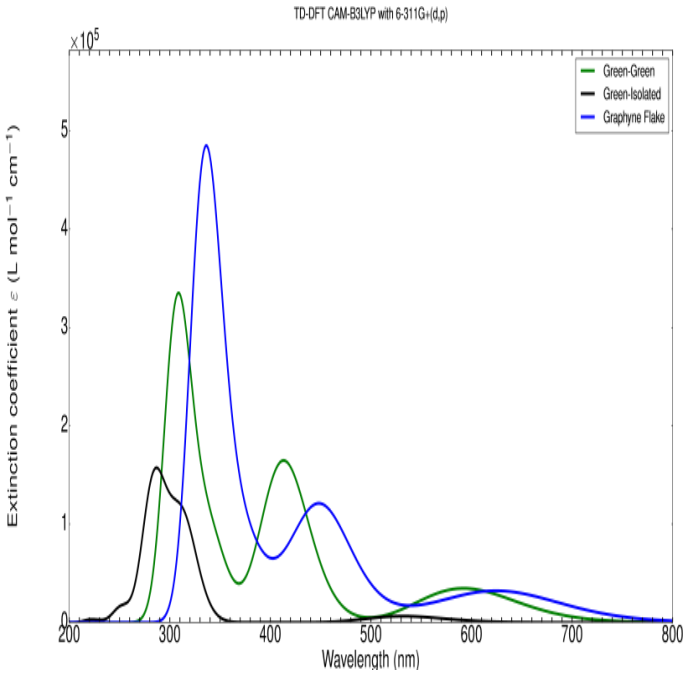

Figure 18: Excitation energies for the Graphyne flake, with the green-green segment combination and isolated green segment for comparison

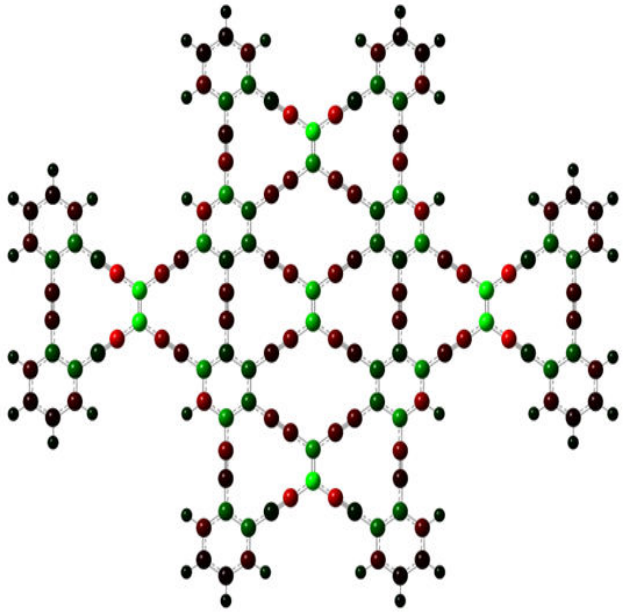

Figure 17: Calculated APT charge population for the neutral Graphyne flake. Colour range going from Green to Red with the values -0.496 to 0.496, respectively

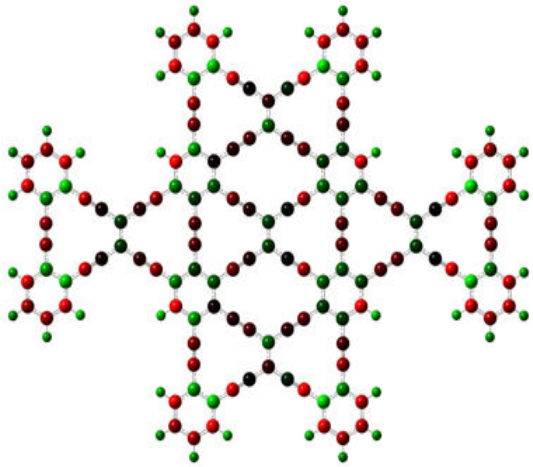

Figure 19: Calculated charge population for the negative charged Graphyne flake (-2). Colour range going from Green to Red with the values -0.240 to 0.240 respectively

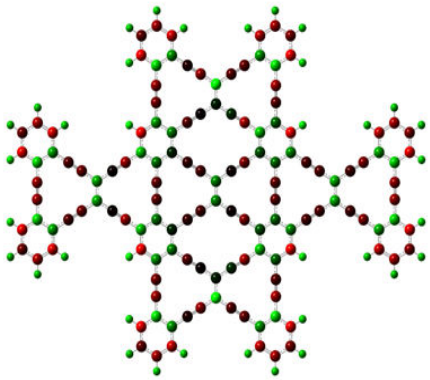

Figure 20: Calculated charge population for the positive charged Graphyne flake (+2). Colour range going from Green to Red with the values -0.222 to 0.222 respectively

6. Graphyne ”Flake”

To further investigate the charge population presented in the previous section, a new structure is proposed. The structure is not one that has been synthesized, but merely an attempt to see how the charge population would change if the system increased in width as well. In the following the structure will be referred to as a *Graphyne Flake*, the structure of the flake was made by using the green segment as starting block. Attaching similar structures, of that of the green segment, to each of the four sides resulted in the flake structure seen in Figure 16. Utilizing this new structure a further investigation of the absorption and charge properties was performed.

6.1. Partial charge distribution of the Graphyne ”flake”

We will consider the partial charges in the flake structure, which is presented in Figure 17. The partial charge distribution shows a charge distribution of ±0.496, which is very similar to what was observed for the isolated segments in the previous section. Regarding the charge localization in the molecule, it was once again observed that the positive partial charge is concentrated on the double bonded carbons in between the benzene rings. While the negative partial charges are placed upon the four carbons surrounding the partial positive carbons. The flake scenario thus further supports the general partial charge placement theory in the Graphyne segments, which hopefully will be observed in the Graphyne sheet.

6.2. Absorption Spectrum for the Graphyne ”Flake”

The TD-DFT calculation for the flake was done using the functional CAM-B3LYP and the basis set 6-311+G(d,p) as with the other TD-DFT calculations. It was expected to provide an absorption spectrum similar to that of the green-green segment combination as it contains a very similar structure. From Figure 18 this expectation was confirmed, by moving from the isolated green segment to the green-green an intensity increase is observed along with a red shift. There is furthermore observed a new peak as a result of the coupling of the two green segments. Looking at the flake the same peaks as for the green-green combination is observed, while the whole absorption band is red-shifted by approximately 20-30 nm. As such the red-shifting effect observed from increasing the size of the system is once again confirmed, while the increase in intensity as a result of an increase of size is also observed for the flake. However, as observed previously the increase in one absorption band results in a decrease in another. As a result the flake structure allows for a high signal to be obtained for the 300-400 nm absorption band, while having a drastically smaller signal for the 400-500 nm absorption band.

6.3. Addition of Charge to the System

Applying a charge of -2 to the Graphyne flake, as seen on Figure 19, a very similar tendency as for the segments is observed for the partial charge distribution. The charge is in general moved away from the double bonded carbon located in between the four benzene rings. The charge behaviour once again shows a tendency to push the charges onto the benzene rings, and as such onto the hydrogen atoms. It should be noted that the triple bonded carbons only carry a charged when placed close to the edge, while the Flake itself shows an general tendency of pushing all charges towards the edges for the negative case, this results in charge distribution of +/- 0.240, which is

half of the neutral case in Fig. 17. Adding a positive charge of +2 to the system once again exhibits an interesting tendency. From Fig. 20 the positive charges are observed to be located at the centre of the molecule on the double bonded carbons. The edge charges are similar to that of the negative case, but the charges are once again for the positive case more de-localized, resulting in the charge distribution of +/- 0.222. This decrease is very small compared with the ones obtained from the segment case (going from -2 to +2 charges), while the same behaviour of carrying changes of the triple bonded carbons is once again observed.

7. Conclusion

The calculations of the excitation energies for the different segments and combinations of segments have shown that the absorption bands are red-shifted as the conjugated system gets larger. Based on a model of a quantum mechanical particle in a two-dimensional box, we are able to obtain excitation energies. For the dimensions of the two-dimension box we have estimated the sizes of the length and width of the conjugated systems. As the area of the conjugation networks gets larger we obtain excitation energies that become more and more red-shifted. Obviously that is related to the solutions of independent electrons moving in a two-dimensional confinement. Therefore we can conclude that the quantum mechanical many electronic structure methods that we have used in the investigation can be qualitatively explained by the use of a simple text book model. On the other hand, the absolute numbers from the two-dimensional model are far away from the rigorous electronic structure calculations and the experimental measured excitation energies.

We also observe that 1) the charge distributions are rather similar for the different segments and 2) the changes of the charge distributions as the total of charges of the segments are change to +2 or -2 are similar for the different segments.

References

[1] Wallace, P. R. The Band Theory of Graphite. *Physical Review* **1947**, *71*, 622–634.

[2] Novoselov, K. S. Electric Field Effect in Atomically Thin Carbon Films. *Science* **2004**, *306*, 666–669.

[3] Phiri, J.; Gane, P.; Maloney, T. C. General overview of graphene: Production, properties and application in polymer composites. *Materials Science and Engineering: B* **2017**, *215*, 9–28.

[4] Pham, V. P.; Jang, H.-S.; Whang, D.; Choi, J.-Y. Direct growth of graphene on rigid and flexible substrates: progress, applications, and challenges. *Chemical Society Reviews* **2017**, *46*, 6276–6300.

[5] Zhong, Y.; Zhen, Z.; Zhu, H. Graphene: Fundamental research and potential applications. *FlatChem* **2017**, *4*, 20–32.

[6] Chakraborty, M.; Hashmi, M. S. J. Wonder material graphene: properties, synthesis and practical applications. *Advances in Materials and Processing Technologies* **2018**, *4*, 573–602.

[7] Liu, M.; Zhang, R.; Chen, W. Graphene-Supported Nanoelectrocatalysts for Fuel Cells: Synthesis, Properties, and Applications. *Chemical Reviews* **2014**, *114*, 5117–5160.

[8] Kong, X.-K.; Chen, C.-L.; Chen, Q.-W. Doped graphene for metal-free catalysis. *Chem. Soc. Rev.* **2014**, *43*, 2841–2857.

[9] Zhu, J.; Yang, D.; Yin, Z.; Yan, Q.; Zhang, H. Graphene and Graphene-Based Materials for Energy Storage Applications. *Small* **2014**, *10*, 3480–3498.

[10] Srivastava, M.; Singh, J.; Kuila, T.; Layek, R. K.; Kim, N. H.; Lee, J. H. Recent advances in graphene and its metal-oxide hybrid nanostructures for lithium-ion batteries. *Nanoscale* **2015**, *7*, 4820–4868.

[11] Huang, X.; Qi, X.; Boey, F.; Zhang, H. Graphene-based composites. *Chem. Soc. Rev.* **2012**, *41*, 666–686.

[12] Premkumar, T.; Geckeler, K. E. Graphene–DNA hybrid materials: Assembly, applications, and prospects. *Progress in Polymer Science* **2012**, *37*, 515–529.

[13] Cranford, S. W.; Buehler, M. J. Mechanical properties of graphyne. *Carbon* **2011**, *49*, 4111–4121.

[14] Ozmaian, M.; Fathizadeh, A.; Jalalvand, M.; Ejtehadi, M. R.; Allaei, S. M. V. Diffusion and self-assembly of C60 molecules on monolayer graphyne sheets. *Scientific Reports* **2016**, *6*, DOI: 10.1038/srep21910.

[15] Wang, G.; Si, M.; Kumar, A.; Pandey, R. Strain engineering of Dirac cones in graphyne. *Applied Physics Letters* **2014**, *104*, 213107.

[16] Kilde, M. D.; Murray, A. H.; Andersen, C. L.; Storm, F. E.; Schmidt, K.; Kadziola, A.; Mikkelsen, K. V.; Hampel, F.; Hammerich, O.; Tykwinski, R. R.; Nielsen, M. B. Synthesis of radiaannulene oligomers to model the elusive carbon allotrope 6, 6, 12-graphyne. *Nature Communications* **2019**, *10*, DOI: 10.1038/s41467-019-11700-0.

[17] Wu, P.; Du, P.; Zhang, H.; Cai, C. Graphyne As a Promising Metal-Free Electrocatalyst for Oxygen Reduction Reactions in Acidic Fuel Cells: A DFT Study. *The Journal of Physical Chemistry C* **2012**, *116*, 20472–20479.

[18] Frisch, M. J.; Trucks, G. W.; Schlegel, H. B.; Scuseria, G. E.; Robb, M. A.; Cheeseman, J. R.; Scalmani, G.; Barone, V.; Petersson, G. A.; Nakatsuji, H.; Li, X.; Caricato, M.; Marenich, A. V.; Bloino, J.; Janesko, B. G.; Gomperts, R.; Mennucci, B.; Hratchian, H. P.; Ortiz, J. V.; Izmaylov, A. F.; Sonnenberg, J. L.; Williams-Young, D.; Ding, F.; Lipparini, F.; Egidi, F.; Goings, J.; Peng, B.; Petrone, A.; Henderson, T.; Ranasinghe, D.; Zakrzewski, V. G.; Gao, J.; Rega, N.; Zheng, G.; Liang, W.; Hada, M.; Ehara, M.; Toyota, K.; Fukuda, R.; Hasegawa, J.; Ishida, M.; Nakajima, T.; Honda, Y.; Kitao, O.; Nakai, H.; Vreven, T.; Throssell, K.; Montgomery Jr., J. A.; Peralta, J. E.; Ogliaro, F.; Bearpark, M. J.; Heyd, J. J.; Brothers, E. N.; Kudin,K. N.; Staroverov, V. N.; Keith, T. A.; Kobayashi, R.; Normand, J.; Raghavachari, K.; Rendell,A. P.; Burant, J. C.; Iyengar, S. S.; Tomasi, J.; Cossi, M.; Millam, J. M.; Klene, M.; Adamo, C.; Cammi, R.; Ochterski, J. W.; Martin, R. L.; Morokuma, K.; Farkas, O.; Foresman, J. B.; Fox, D. J. Gaussian˜16 Revision C.01, Gaussian Inc. Wallingford CT, 2016.

[19] Serr, A.; Boyle, N. O. Convoluting UV-Vis spectra using oscillator strengths. **2017**, DOI: 10.5281/zenodo.820871.

[20] Yanai, T.; Tew, D. P.; Handy, N. C. A new hybrid exchange–correlation functional using the Coulomb-attenuating method (CAM-B3LYP). *Chemical Physics Letters* **2004**, *393*, 51–57.

[21] Huff, G. S.; Gallaher, J. K.; Hodgkiss, J. M.; Gordon, K. C. No single DFT method can predict Raman cross-sections, frequencies and electronic absorption maxima of oligothiophenes. *Synthetic Metals* **2017**, *231*, 1–6.